

GRB 051022: physical parameters and extinction of a prototype dark burst

Evert Rol¹, Alexander van der Horst², Klaas Wiersema², Sandeep K. Patel^{3,4}, Andrew Levan⁵, Melissa Nysewander⁶, Chryssa Kouveliotou^{3,7}, Ralph A. M. J. Wijers², Nial Tanvir¹, Dan Reichart⁸, Andrew S. Fruchter⁶, John Graham^{6,9}, Jan-Erik Ovaldsen¹⁰, Andreas O. Jaunsen¹⁰, Peter Jonker^{11,12,13}, Wilbert van Ham¹⁴, Jens Hjorth¹⁵, Rhaana L. C. Starling¹, Paul T. O'Brien¹, Johan Fynbo¹⁵, David N. Burrows¹⁶, Richard Strom^{2,17}

ABSTRACT

GRB 051022 was undetected to deep limits in early optical observations, but precise astrometry from radio and X-ray showed that it most likely originated in a galaxy at $z \approx 0.8$. We report radio, optical, near infra-red and X-ray observations of GRB 051022. Using the available X-ray and radio data, we model the afterglow and calculate the energetics of the afterglow, finding it to be an order of magnitude lower than that of the prompt emission. The broad-band modeling also allows us to precisely define various other physical parameters and the minimum required amount of extinction, to explain the absence of an optical afterglow. Our observations suggest a high extinction, at least 2.3 magnitudes in the infrared (J) and at least 5.4 magnitudes in the optical (U) in the host-galaxy restframe. Such high extinctions are unusual for GRBs, and likely indicate a geometry where our line of sight to the burst passes through a dusty region in the host that is not directly co-located with the burst itself.

Subject headings: gamma rays: bursts — dust, extinction

1. Introduction

Dark gamma-ray bursts (GRBs) — at the most basic level those without optical afterglows — are a long-standing issue in GRB observations. Although in many cases the non-detection of an afterglow at optical wavelengths may simply be due

¹Department of Physics and Astronomy, University of Leicester, University Road, Leicester, LE1 7RH, United Kingdom; evert.rol@star.le.ac.uk

²Astronomical Institute, University of Amsterdam, Kruislaan 403, NL-1098 SJ Amsterdam, The Netherlands

³National Space Science and Technology Center, 320 Sparkman Drive, Huntsville, AL-35805, USA

⁴Optical Sciences Corporation, 6767 Old Madison Pike, Suite 650, Huntsville, AL, 35806

⁵Department of Physics, University of Warwick, Coventry, CV4 7AL, UK

⁶Space Telescope Science Institute, 3700 San Martin Drive, Baltimore, MD-21218

⁷NASA Marshall Space Flight Center

⁸Department of Physics and Astronomy, University of North Carolina at Chapel Hill, Campus Box 3255, Chapel Hill, NC-27599, USA

⁹Department of Physics and Astronomy, Johns Hopkins University, 3400 North Charles St., Baltimore, MD-21218

¹⁰Institute of Theoretical Astrophysics, University of Oslo, P.O.Box 1029, Blindern, N-0315 Oslo, Norway

¹¹SRON, Netherlands Institute for Space Research, Sor-

bonnelaan 2, NL-3584 CA Utrecht, The Netherlands

¹²Harvard-Smithsonian Center for Astrophysics, 60 Garden Street, Cambridge, MA-02138, Massachusetts, USA

¹³Astronomical Institute, Utrecht University, P.O.Box 80000, 3508 TA, Utrecht, The Netherlands

¹⁴Department of Astrophysics, Radboud University Nijmegen, P.O.Box 9010, NL-6500 GL Nijmegen, The Netherlands

¹⁵Dark Cosmology Centre, Niels Bohr Institute, University of Copenhagen, Juliane Maries Vej 30, DK-2100 Copenhagen Ø, Denmark

¹⁶Penn State University, State College, PA 16801, USA

¹⁷ASTRON, P.O. Box 2, NL-7990 AA Dwingeloo, Netherlands

to an insufficiently deep search, or one which takes place at late times (e.g. Fynbo et al. 2001), a subset of GRBs with bright X-ray afterglows remains undetected despite prompt and deep optical searches (e.g. Groot et al. 1998) and directly implies suppression of the optical light.

There are several plausible explanations for this, the most likely being that the burst is at high redshift, such that the Ly-alpha break has crossed the passband in question, or that there is high extinction in the direction of the GRB. Examples of both have been found, with a small number of GRBs at $z > 5$ appearing as V and R band dropouts (e.g. Jakobsson et al. 2006b; Haislip et al. 2006) and some GRB afterglows appearing very red at lower redshift, due to effects of extinction (e.g. Levan et al. 2006; Rol et al. 2007).

Identification of GRBs at very high redshifts is the key to using them as cosmological probes. The proportion of bursts exhibiting high dust extinction is also interesting from the point of view of estimating the proportion of star formation that is dust enshrouded, as well as understanding the environments which favor GRB production (Trentham et al. 2002; Tanvir et al. 2004).

The detection and follow-up of dark bursts at other wavelengths is essential, as it enables 1) the modeling of the afterglow, deriving estimates of the extinction and energies involved, potentially providing information about the direct burst environment, 2) pinpointing the burst position in the host, to enable late-time high resolution imaging and the detection of dust enhanced regions in the host, and 3) determination of the properties of the GRB host itself, such as the SFR and average host-galaxy extinction.

The High Energy Transient Explorer 2 mission (HETE-2; Ricker et al. 2003) detected and located an unusually bright gamma-ray burst (Olive et al. 2005) with its three main instruments, the French Gamma Telescope (FREGATE), the Wide field X-ray monitor (WXM) and the Soft X-ray Camera, (SXC), on October 22, 2005. A 2.5 arcminute localization was sent out within minutes, enabling prompt follow-up observations (e.g. Torii 2005; Schaefer 2005); a target-of-opportunity observation was also performed with *Swift*. Details of the HETE-2 observations can be found in Nakagawa et al. (2006).

The *Swift* observations resulted in the detection of a single fading point source inside the SXC error region, which was consequently identified as the X-ray afterglow of GRB 051022 (Racusin et al. 2005a). However, optical and near infra-red (nIR) observations failed to reveal any afterglow to deep limits, while radio and millimeter observations with the Very Large Array (VLA), the Westerbork Synthesis Radio Telescope (WSRT) and the Plateau de Bure Interferometer detected the radio counterpart (Cameron & Frail 2005; Van der Horst et al. 2005; Bremer et al. 2005). The position coincides with its likely host galaxy (Berger & Wyatt 2005) at a redshift of $z = 0.8$ (Gal-Yam et al. 2005).

In this paper, we describe our X-ray, optical, nIR and radio observations of GRB 051022. The outline of the paper is as follows: in Section 2 we describe our observations, data reduction and initial results. In Section 3, we analyze these results and form our afterglow picture, which is discussed in Section 4. Our findings are summarized in Section 5.

In the following, we have used $F \propto \nu^{-\beta} t^{-\alpha}$ in our definition of α and β . We assume a cosmology with $H_0 = 71 \text{ kms}^{-1} \text{ Mpc}^{-1}$, $\Omega_M = 0.27$ and $\Omega_\Lambda = 0.73$. All quoted errors in this paper are 1 sigma (68%) errors.

2. Observations and data reduction

2.1. X-ray observations

X-ray observations were performed with the *Swift* X-Ray Telescope (XRT) and the Chandra X-ray Observatory (CXO).

The XRT started observing the afterglow of GRB 051022 3.46 hours after the HETE-2 trigger, for a total effective integration time of 137 ks between October 22 and November 6.

Observations were performed in Photon Counting (PC) mode, the most sensitive observing mode. We reduced the data using the *Swift* software version 2.6 in the HEASoft package version 6.2.0. Data were obtained from the quick-look site and processed from level 1 to level 2 FITS files using the `xrtpipeline` tool in its standard configuration. The first two orbits (until 2.1×10^4 seconds post burst) show pile-up and were therefore extracted with an annular rather than circular

region, with an inner radius of 19 and 12'' for orbits 1 and 2, respectively, and an outer radius of 71''. Orbits 3 – 7 ($2.4 \times 10^4 - 4.9 \times 10^4$ seconds) were extracted with a circular region of 71'' radius, and later orbits were extracted using a 47'' radius circle instead. The data for the light curve were extracted between channels 100 and 1000, corresponding to 1 and 10 keV, respectively; while the commonly used range is 0.3 – 10 keV, the large absorption prevents the detection of any data from the source below 1 keV. Otherwise, the procedure is similar to that described in Evans et al. (2007).

Observations with the CXO started on October 25, 2005, 21:14:20, 3.34 days after the HETE trigger, for a total integration time of 20 ks (Patel et al. 2005). Data were reduced in a standard fashion with the CIAO package.

We performed astrometry by matching X-ray sources with an optical *R*-band image that was astrometrically calibrated to the 2MASS catalog. Our CXO position is RA, Dec = 23:56:04.115, +19:36:24.04 (J2000), with positional errors of 0.33'' and 0.12'' for the Right Ascension and Declination, respectively. This puts the afterglow within 0.5'' of the center of its host galaxy.

We modeled the XRT spectra with an absorbed power law in XSpec (Arnaud 1996), using data from the first seven orbits. A good fit ($\chi^2/\text{d.o.f.} = 87.2/99$) was obtained with a resulting spectral energy index of $\beta = 1.00 \pm 0.12$ and excess absorption (at $z = 0.8$ and for assumed Galactic abundances) of $N_{\text{H}} = (2.82 \pm 0.46) \times 10^{22} \text{ cm}^{-2}$ on top of the estimated Galactic absorption at this position ($N_{\text{H}} = 4.06 \times 10^{20} \text{ cm}^{-2}$, Dickey & Lockman 1990). The CXO data are fully in agreement with these values, showing no change in the spectrum over time between 0.3 and 3.3 days after the burst. The absorption measured is far less than that measured by the HETE team in their prompt data, $N_{\text{H}} = (8.8_{-1.8}^{+1.9}) \times 10^{22} \text{ cm}^{-2}$ (Nakagawa et al. 2006). This could indicate a change in absorption between the early (prompt) measurements and those at the time of the XRT observations. For the prompt emission spectrum, however, the values found by Konus-Wind (Golenetskii et al. 2005) are rather different than those found by HETE-2, and may be the result of the lower energy cut-off for FREGATE compared to Konus-wind. Alternatively, the fact that these spectra are an average over the whole emission period may also result in

incorrect model parameters. In the two last cases, the N_{H} in the prompt emission could be as low as the XRT value and still produce an equally well fit, but with slightly different model parameters.

For the XRT data, Butler et al. (2005a) and Nakagawa et al. (2006) find a value somewhat higher than our value ($4.9 \times 10^{22} \text{ cm}^{-2}$ and $5.3 \times 10^{22} \text{ cm}^{-2}$ respectively, when scaled by $(1+z)^3$, Gunn & Peterson 1965). This difference could be explained by a different count-binning or an updated XRT calibration used in our modeling.

The XRT light curve count rates have been converted to 1–10 keV fluxes using the results from our spectral modeling and calculating the ratio of the flux and count rate at the logarithmic center of the orbits. The 1 – 10 keV CXO flux was derived using the actual spectral fit.

A broken power law fit to the X-ray light curve results in $\alpha_1 = 1.16 \pm 0.06$, $\alpha_2 = 2.14 \pm 0.17$ and a break time of 110_{-23}^{+21} ks, or around 1.27 days. The difference between α_1 and α_2 , and the fact that the spectral slope does not change across the break (the CXO measurement is past the break), are highly indicative that the observed break in the light curve is a jet break. In Section 3.1, we perform full modeling of the afterglow using the fireball model, indeed resulting in a jet-break time t_j that agrees reasonably well with the break time as determined from only the X-rays. We point out that our value for t_j is different than that cited in Racusin et al. (2005b), largely because their measurement of t_j was based on a preliminary XRT light curve.

2.2. Optical and near infra-red observations

Observations were obtained in *Z* and *R*-band with the William Herschel Telescope (WHT) using the Auxiliary Port and the Prime Focus Imaging Camera, respectively, in *r'i'z'* with the Gemini South telescope using the GMOS instrument, in *JHK_s* with the Wide Field Camera on the United Kingdom InfraRed Telescope (UKIRT), in *BVRI* with the DFOSC instrument on the Danish 1.54m telescope and in *J* and *K_s* with the Southern Astrophysical Research (SOAR) telescope using OSIRIS. The optical data were reduced in a standard fashion using the *ccdproc* package within the IRAF software (Tody 1986), whereas the SOAR

data were reduced using the *cirred* package within IRAF. The UKIRT data were reduced using the standard pipeline reduction for WFCAM.

Photometric calibration was done using the calibration provided by Henden (2005) for Johnson-Cousins filters. For the $r'i'z'$ GMOS filters, we converted the magnitudes of the calibration stars provided by Henden to the Sloan filter system using the transformations provided by Jester et al. (2005), and verified by the published GMOS zero points. The WHT Z -band was calibrated using the spectroscopic standard star SP2323+157. Calibration of the infrared JHK magnitudes was done using the 2MASS catalog (Skrutskie et al. 2006).

No variable optical source was found at the position of the X-ray and radio afterglow. For the early epoch images (< 1 day post burst), we estimated a limiting magnitude by performing image subtraction between this and a later image using the ISIS image subtraction package (Alard 2000). To this end, artificial low signal-to-noise sources were added onto the images, with a Gaussian PSF matched in size to the seeing (some artificial sources were added on top of existing sources, e.g. galaxies, some on the background sky). We determined our upper limit to be the point where we could retrieve 50% of the artificial sources in the subtracted image. This assumes that the change in brightness of any point source on top of the host galaxy is sufficient to be seen in such a subtracted image. With the difference in time between the epochs, this seems a reasonable assumption (for example, for a source fading with a shallow power law like slope of $F \propto t^{-0.5}$, the magnitude difference between the two WHT Z -band observations is ≈ 0.6 magnitudes).

Photometry of the host galaxy has been performed using aperture photometry, with an aperture 1.5 times the seeing for each image, estimated from the measured FWHM of the PSF for point sources in the images.

Table 1 shows the log of our optical/nIR observations, while Table 2 shows the upper limits for any optical/nIR afterglow.

2.3. Radio observations

Radio observations were performed with the WSRT at 8.4 GHz, 4.9 GHz and 1.4 GHz. We

used the Multi Frequency Front Ends (Tan 1991) in combination with the IVC+DZB back end¹ in continuum mode, with a bandwidth of 8x20 MHz. Gain and phase calibrations were performed with the calibrators 3C 286 and 3C 48, although at one 8.4 GHz measurement 3C 147 was used. Reduction and analysis were performed using the MIRIAD software package². The observations are detailed in Table 3. In our modeling described in section 3.1 we have also used the VLA radio detection at 8.5 GHz from Cameron & Frail (2005).

3. Analysis

3.1. Broadband modeling

We have performed broadband modeling of the X-ray and radio measurements, using the methods presented in van der Horst et al. (2007). In our modeling we assume a purely synchrotron radiation mechanism.

The relativistic blastwave causing the afterglow accelerates electrons to relativistic velocities, which gives rise to a broadband spectrum with three characteristic frequencies: the peak frequency ν_m , corresponding to the minimum energy of the relativistic electrons that are accelerated by the blastwave, the cooling frequency ν_c , corresponding to the electron energy at which electrons lose a significant fraction of their energy by radiation on a timescale that is smaller than the dynamical timescale, and the self-absorption frequency ν_a , below which synchrotron self-absorption produces significant attenuation. The broadband spectrum is further characterized by the specific peak flux $F_{\nu, \max}$ and the slope p of the electron energy distribution.

The dynamics of the relativistic blastwave determine the temporal behavior of the broadband synchrotron spectrum, i.e. the light curves at given frequencies. At first the blastwave is extremely relativistic, but is decelerated by the surrounding medium. When the Lorentz factor Γ of the blastwave becomes comparable to θ_j^{-1} , where θ_j is the opening angle of the jet, the jet starts to spread sideways. At that time, t_j , the temporal behavior of the broadband spectrum changes (see e.g. Rhoads 1997).

¹See sect. 5.2 at <http://www.astron.nl/wsrt/wsrtGuide/node6.html>

²<http://www.atnf.csiro.au/computing/software/miriad>

TABLE 1
OVERVIEW OF OPTICAL OBSERVATIONS

Start date	ΔT (average) (days)	exposure time (seconds)	filter	seeing (arcsec)	telescope & instrument
2005-10-22T23:25:14	0.4287	1800	Z	0.8	WHT + API
2005-10-23T00:22:33	0.4684	1620	J	1.2	SOAR + OSIRIS
2005-10-23T00:56:00	0.4917	1620	K_s	1.3	SOAR + OSIRIS
2005-10-23T00:48:03	0.5144	1920	i'	0.6	Gemini South + GMOS
2005-10-23T01:07:53	0.5288	1920	r'	0.6	Gemini South + GMOS
2005-10-23T01:27:46	0.5426	1920	z'	0.5	Gemini South + GMOS
2005-10-23T06:31:03	0.7525	720	J	1.4	UKIRT + WFCAM
2005-10-23T06:36:39	0.7526	360	H	1.3	UKIRT + WFCAM
2005-10-23T06:47:59	0.7604	360	K	1.3	UKIRT + WFCAM
2005-10-23T21:15:57	1.3389	1200	Z	1.0	WHT + API
2005-10-24T09:35:10	1.8467	720	K	0.3	UKIRT + WFCAM
2005-10-25T01:34:03	2.5181	1602	K_s	1.3	SOAR + OSIRIS
2005-10-25T02:13:18	2.5454	720	J	1.2	SOAR + OSIRIS
2005-10-25T02:22:02	2.5698	1920	r'	1.1	Gemini South + GMOS
2005-10-25T02:39:59	2.5792	1440	z'	1.2	Gemini South + GMOS
2005-10-26T00:36:58	3.4785	1800	R	1.4	WHT+PFIP
2005-10-26T02:48:06	3.5695	600	Gunn i	1.4	DK1.54m + DFOSC
2005-10-26T03:23:35	3.5942	600	R	1.9	DK1.54m + DFOSC
2005-10-27T01:01:04	4.4952	600	B	2.3	DK1.54m + DFOSC
2005-10-27T02:59:20	4.5773	600	R	1.6	DK1.54m + DFOSC
2005-10-27T02:00:48	4.5367	600	V	1.8	DK1.54m + DFOSC
2005-10-28T02:18:38	5.5491	600	i	1.4	DK1.54m + DFOSC
2005-10-30T02:32:59	7.5590	600	B	1.8	DK1.54m + DFOSC
2005-10-30T04:18:30	7.6323	600	U	1.8	DK1.54m + DFOSC
2005-10-30T01:33:57	7.5180	600	V	1.4	DK1.54m + DFOSC
2005-10-31T03:19:05	8.5910	600	B	1.0	DK1.54m + DFOSC
2005-10-31T01:03:40	8.4970	600	R	1.0	DK1.54m + DFOSC
2005-10-31T02:10:02	8.5431	600	V	1.0	DK1.54m + DFOSC
2005-11-01T01:52:57	9.5312	600	R	0.9	DK1.54m + DFOSC
2005-11-02T02:04:47	10.539	600	V	1.2	DK1.54m + DFOSC
2005-11-03T01:10:34	11.502	600	B	1.2	DK1.54m + DFOSC
2005-11-07T01:25:30	15.512	600	Gunn i	1.4	DK1.54m + DFOSC
2005-11-08T01:40:48	16.523	600	Gunn i	1.4	DK1.54m + DFOSC

TABLE 2
LIMITING MAGNITUDES

filter	limiting magnitude ^a	ΔT (average) days	frequency Hz	specific flux ^b μJy
K_s	> 20.0	0.4917	$1.40 \cdot 10^{14}$	< 6.82
J	> 20.3	0.4684	$2.40 \cdot 10^{14}$	< 12.3
Z	> 22.9	0.4287	$3.43 \cdot 10^{14}$	< 2.66
z'	> 23.5	0.5426	$3.36 \cdot 10^{14}$	< 1.53
r'	> 25.3	0.5288	$4.76 \cdot 10^{14}$	< 0.305

^aSee text for the definition of the limiting magnitude.

^bSpecific fluxes have been corrected for a Galactic extinction value of $E_{B-V} = 0.04$ (Schlegel et al. 1998), and converted from magnitudes using the calibration by Tokunaga & Vacca (2005) for the JK_s filters; the other filters are on the magnitude AB-system (Oke & Gunn 1983)

TABLE 3
OVERVIEW OF WSRT RADIO OBSERVATIONS

Start date	ΔT (average) (days)	integration time (hours)	frequency (GHz)	specific flux (μJy)
2005-11-04T18:14:24	13.37	4.0	8.5	38 ± 132
2005-11-08T14:19:41	17.19	7.0	8.5	28 ± 97
2005-10-23T15:20:10	1.19	5.0	4.9	281 ± 32
2005-10-24T15:17:17	2.22	6.2	4.9	342 ± 34
2005-10-25T15:12:58	3.30	5.4	4.9	143 ± 30
2005-10-28T18:33:08	6.40	8.5	4.9	91 ± 28
2005-10-30T18:00:00	8.32	5.8	4.9	138 ± 28
2005-11-01T18:00:00	10.38	8.9	4.9	169 ± 28
2005-11-04T17:31:12	13.37	4.6	4.9	70 ± 34
2005-10-25T15:56:10	3.33	5.4	1.4	8 ± 78

We fit our data to six parameters: ν_c , ν_m , ν_a , $F_{\nu, \max}$, p and t_j . From these parameters and the redshift of the burst, $z = 0.8$, we can find the physical parameters governing the blastwave and its surroundings: the blastwave isotropic equivalent energy E_{iso} , the jet opening angle θ_j , the collimation corrected blastwave energy E_{jet} , the fractional energy densities behind the relativistic shock in electrons and in the magnetic field, ϵ_e and ϵ_B respectively, and the density of the surrounding medium. The meaning of the latter parameter depends on the density profile of the surrounding medium. For a homogeneous circumburst medium, we simply determine the density n . For a massive stellar wind, where the density is proportional to R^{-2} with R the distance to the GRB explosion center, we obtain the parameter A_* , which is the ratio of the mass-loss rate over the terminal wind velocity of the GRB progenitor.

Our modeling results are shown in Table 4, for both the homogeneous external medium and the stellar wind environment. The light curves for the best fit parameters are shown in Figure 1. We have performed Monte Carlo simulations with synthetic data sets in order to derive accuracy estimates of the best fit parameters, which are also given in the table. It is evident from the results that our six fit parameters are reasonably well constrained in both cases for the circumburst medium. The derived physical parameters are also well constrained, except for ϵ_e and ϵ_B . The values we find for both the isotropic and the collimation corrected energy, are similar to those found for other bursts; this is also true for p . See e.g. Panaitescu & Kumar (2001) and Yost et al. (2003). The jet opening angle and the density of the surrounding medium are quite small, but both not unprecedented. The jet-break time t_j is somewhat smaller than estimated in Section 2.1, but both estimates have relatively large errors, likely because of the lack of (X-ray) data around the jet-break time.

With the absence of optical light curves, it is not possible to discriminate between the two different circumburst media. This is mainly due to the fact that the X-ray band lies above both ν_m and ν_c , in which case the slopes of the light curves do not depend on the density profile of the circumburst medium (even at 0.15 days, back-extrapolating ν_c from Table 4 results in its value being below the X-ray band). The χ^2_{red} is some-

what better for the stellar wind case, but the homogeneous case cannot be excluded. From the X-ray light curve, however, one can conclude that the density profile of the medium does not change between approximately 0.15 and 12 days after the burst. If there were a transition from a stellar wind to a homogeneous medium, the X-ray flux has to rise or drop significantly, unless the densities are fine-tuned at the transition point (Pe’er & Wijers 2006). From the fact that the medium does not change during the X-ray observations, one can draw conclusions on the distance of the wind termination shock of the massive star: if one assumes that the medium is already homogeneous at ≈ 0.15 days, the wind termination shock position is at $R_w \lesssim 9.8 \cdot 10^{17}$ cm (0.32 pc); if the circumburst medium is a stellar wind up to ≈ 12 days after the burst, $R_w \gtrsim 1.1 \cdot 10^{19}$ cm (3.7 pc).

3.2. The non-detection of the optical afterglow

It is quickly seen that GRB 051022 falls into the category of the so-called “dark bursts”. Using, for example, the quick criterion proposed by Jakobsson et al. (2004), we find $\beta_{OX} < -0.05$ at 12.7 hours after the burst using the Gemini r' band observation, well below the proposed limit of $\beta_{OX} < 0.5$. A more precise criterion would combine the available spectral and temporal parameters of the X-ray afterglow, allow all valid combinations, and from that infer the range of possible optical magnitudes from the X-rays (see e.g. Rol et al. 2005). This is, in fact implied in our previous modeling: the modeled specific fluxes corresponding to the band and epoch of our optical and nIR upper limits are listed in Table 5 (see also Table 2).

While the values in this table are given for local extinction, not K-corrected to $z = 0.8$, it is immediately obvious that our K-band observations put a stringent constraint on the required extinction directly surrounding the burst.

To estimate the amount of local extinction in the host galaxy, we have modeled the nIR to X-ray spectrum around 0.5 days after the burst, considering 3 different extinction curves: those of the Milky Way (MW), the Large Magellanic Cloud (LMC) and the Small Magellanic Cloud (SMC), from Pei (1992), with R_V of 3.08, 3.16 and 2.93, respectively.

TABLE 4

RESULTS OF BROADBAND MODELING FOR BOTH A HOMOGENEOUS EXTERNAL MEDIUM AND A MASSIVE STELLAR WIND. THE BEST FIT PARAMETERS ARE SHOWN TOGETHER WITH ACCURACY ESTIMATES FROM MONTE CARLO SIMULATIONS WITH SYNTHETIC DATA SETS. THE CHARACTERISTIC FREQUENCIES OF THE SYNCHROTRON SPECTRUM AND THE SPECIFIC PEAK FLUX ARE GIVEN AT t_j .

Parameter	Homogeneous	Stellar wind
$\nu_c(t_j)$	$(1.45^{+1.12}_{-0.23}) \cdot 10^{17}$ Hz	$(2.84^{+0.32}_{-1.30}) \cdot 10^{17}$ Hz
$\nu_m(t_j)$	$(3.50^{+2.26}_{-1.47}) \cdot 10^{11}$ Hz	$(2.90^{+2.03}_{-1.15}) \cdot 10^{11}$ Hz
$\nu_a(t_j)$	$(4.56^{+2.85}_{-3.08}) \cdot 10^9$ Hz	$(2.68^{+2.17}_{-1.60}) \cdot 10^9$ Hz
$F_{\nu, \max}(t_j)$	888^{+52}_{-109} μ Jy	694^{+30}_{-240} μ Jy
p	$2.06^{+0.19}_{-0.05}$	$2.10^{+0.08}_{-0.09}$
t_j	$0.96^{+0.40}_{-0.28}$ days	$1.06^{+0.41}_{-0.11}$ days
θ_j	$3.39^{+2.02}_{-2.27}$ deg	$2.30^{+1.09}_{-0.85}$ deg
E_{iso}	$(5.23^{+1.13}_{-1.69}) \cdot 10^{52}$ erg	$(28.2^{+31.0}_{-10.4}) \cdot 10^{52}$ erg
E_{jet}	$(0.917^{+0.655}_{-0.512}) \cdot 10^{50}$ erg	$(2.27^{+2.25}_{-0.79}) \cdot 10^{50}$ erg
ε_e	$0.247^{+1.396}_{-0.212}$	$0.0681^{+0.3951}_{-0.0348}$
ε_B	$(7.63^{+42.57}_{-6.30}) \cdot 10^{-3}$	$(8.02^{+28.18}_{-7.17}) \cdot 10^{-3}$
n	$(1.06^{+9.47}_{-1.04}) \cdot 10^{-2}$ cm $^{-3}$...
A_*^a	...	$(2.94^{+6.98}_{-2.11}) \cdot 10^{-2}$
χ^2_{red}	1.9	1.5

^aThe parameter A_* is a measure for the density in the case of a stellar wind environment, being the ratio of the mass-loss rate over the terminal wind velocity, and here given in units of 10^{-5} Solar masses per year divided by a wind velocity of 1000 km/s (see van der Horst et al. 2007).

TABLE 5

UPPER LIMITS COMPARED TO MODEL SPECIFIC FLUX CALCULATIONS. THE INFERRED LOWER LIMITS ON THE EXTINCTION ARE GIVEN IN THE OBSERVERS FRAME. THE E_{B-V} VALUES ARE GIVEN FOR A GALACTIC EXTINCTION CURVE ($R_V = 3.08$), AND ARE FOR ILLUSTRATIVE PURPOSES; SEE THE COMMENTS AT THE END OF SECTION 3.2.

filter	upper limit (μ Jy)	homogeneous density profile			stellar wind density profile		
		modeled specific flux (μ Jy)	extinction (mag.)	E_{B-V}	modeled specific flux (μ Jy)	extinction (mag.)	E_{B-V}
K_s	< 6.82	93.1	2.84	7.74	57.2	2.31	6.29
J	< 12.3	117	2.44	2.71	74.1	1.95	2.16
Z	< 2.66	103	3.97	2.58	67.8	3.52	2.29
r'	< 0.305	74.5	5.97	2.17	44.4	5.41	1.97
z'	< 1.53	87.7	4.40	2.97	51.9	3.83	2.59

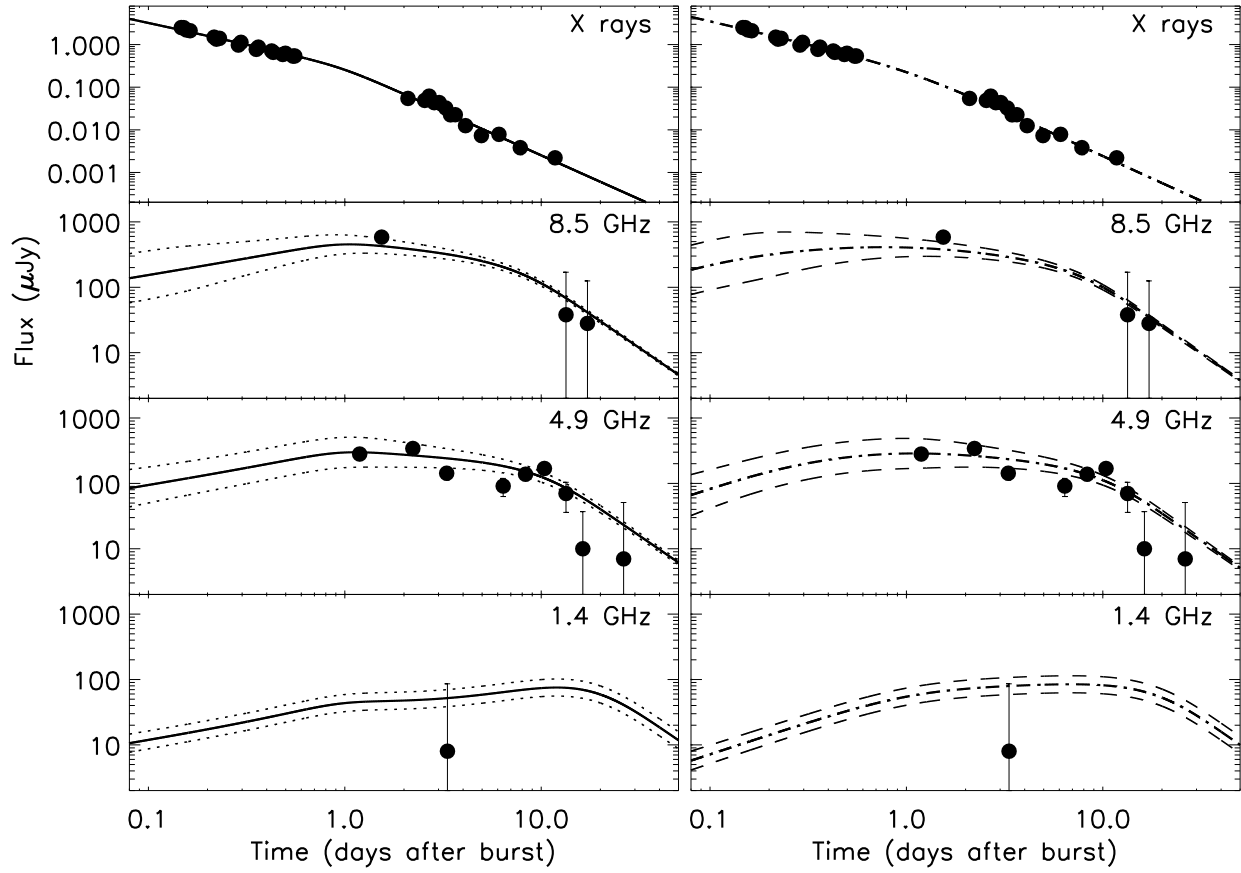


Fig. 1.— Fit results for a homogeneous circumburst medium (left panel) and a massive stellar wind (right panel). The solid and dash-dotted lines are the best model fits, and the dotted and dashed lines indicate the predicted rms scatter due to interstellar scintillation; see the appendix for further details. Also included in the figure (and modeling) is the reported VLA 8.5 GHz detection (Cameron & Frail 2005, left-most point in the 8.5 GHz subplot).

For this, we used the unabsorbed XRT flux obtained from the spectral fit to orbits 3 – 7 (which do not contain piled-up data), and fixed the energy spectral slope in the X-rays at $\beta = 1$ (also from the X-ray spectral fit). The optical specific fluxes were scaled to the logarithmic mid-observation time of the X-ray observations with an assumed $\alpha = 1.16$ decline. This estimated optical decay is derived from the pre-break X-ray decay value, allowing for the cooling break between the two wavelength regions, and averaging the two possible values for $\alpha_X - \alpha_{\text{opt}}$ (-0.25 and 0.25). We can further put the most stringent constraint on the broken power law spectral shape, by setting the spectral break just below the X-rays, at 1.8×10^{17} Hz, which follows from our previous broad-band modeling. Our results indicate that, for the aforementioned extinction curves, a local extinction of $E_{B-V} \approx 7$ (for all three extinction curves) is necessary to explain the K -band upper limit.

We can relate the resulting N_H from our X-ray spectral fits to any local E_{B-V} , using the relations found in Predehl & Schmitt (1995), Fitzpatrick (1985) and Martin et al. (1989) for $N(HI)/E_{B-V}$, and adjusting the metallicity in our X-ray absorption model accordingly. We obtain $E_{B-V} = 7.5, 1.54$ and 0.84 for a MW, LMC and SMC extinction curve respectively, with the MW value showing the best agreement with our findings for optical extinction (both Nakagawa et al. 2006 and Butler et al. 2005b find E_{B-V} values roughly twice as high here, for a MW extinction curve only, since their N_H estimate is larger than ours). This, obviously, depends on the assumption that the MW (or otherwise, LMC or SMC) extinction curves are valid models to compare with our observed data here. Since these data happen to originate from just one sight line in a galaxy, this may very well not be the case. Further, even if the extinction curve is correct, the actual value of R_V may be rather different for the host galaxy. Finally, the $E_{B-V} - N_H$ relations show a rather large scatter, especially at higher column densities, nor is the N_H always derived using X-ray spectroscopy. Our above results are therefore approximations, which are useful to compare with other (GRB host) studies, but should be taken with the necessary caution.

3.3. The host galaxy of GRB 051022

Using the optical data described above, we fit the SED of the host of GRB 051022 using the HyperZ program³ developed by Bolzonella et al. (2000). The photometry of the host has been performed using `apphot` within IRAF, in an aperture 1.5 times the estimated seeing in the different exposures. The results are reported in Table 6 (see also Ovaldsen et al. 2007). The range of photometric magnitudes reported in this paper provides one of the most complete broadband optical datasets of a GRB host galaxy to date. We fit using the eight synthetic galaxy templates provided within HyperZ at the redshift of the host, and find that the host galaxy is a blue compact galaxy of type irregular, with a dominant stellar population age of ≈ 20 Myr, similar to other long GRB hosts (Christensen et al. 2005). A moderate amount of extinction of $A_V \approx 1$ mag is required to fit the SED, with an SMC-type extinction curve providing a best fit, and the luminosity of the host is approximately $1.5 L_*$ (assuming $M_{*,B} = -21$); these findings are in full agreement with Castro-Tirado et al. (2006). The amount of extinction in the line of sight towards the GRB required to suppress the optical light of the afterglow to the observed limits is clearly higher than the A_V value found from the host SED: $A_V = 4.4$ magnitudes towards the GRB, estimated from blueshifting our measured (observer frame) z' band extinction to $z = 0.8$. The host galaxy SED extinction is, however, an average value derived from the integrated colors of the host.

The host of GRB 051022 is located in a field crowded with galaxies of various Hubble types. We perform photometry on several galaxies close to the GRB host (within 1 arcminute) to investigate the possibility that the high star formation rate seen in the optical (Castro-Tirado et al. 2006 report an SFR of $\approx 20 M_\odot \text{yr}^{-1}$) is induced by a recent interaction with one of the neighboring galaxies. As formation of high mass stars has also been observed to occur in dusty regions in merging systems (see e.g. Lin et al. 2007), this could help to explain the excess optical extinction towards GRB 051022. We performed HyperZ fits to these galaxies, and find that none of them is well fit by a photometric redshift of $z \approx 0.8$. Particularly

³See <http://webast.ast.obs-mip.fr/hyperz>

TABLE 6
MEASURED HOST GALAXY MAGNITUDES

filter	magnitude	magnitude error
K	18.40	0.04
K_s	18.36	0.09
H	19.42	0.09
J	19.92	0.05
Z^a	21.41	0.05
z'	21.30	0.04
i'	21.77	0.01
r'	22.04	0.01
R	21.84	0.09
V	22.30	0.04
B	22.75	0.02
U	$> 21.3^b$...

^aAB magnitude

^b5- σ upper limit

the two galaxies closest to the GRB host galaxy are not compatible with a redshift 0.8, and show best fits with photometric redshifts of $z \approx 0.2 - 0.25$. Out of the sample of six galaxies close to the GRB host we find that four have best-fit photometric redshifts in the range $0.20 - 0.25$, making it unlikely that a possible overdensity of galaxies near the host galaxy is due to a cluster or galaxy group at the host redshift.

4. Discussion

The issue of non-detected (“dark”) GRB afterglows has received significant interest ever since the discovery of the first GRB afterglow, starting with the non-detection of GRB 970828 to very deep limits (Groot et al. 1998; Odewahn et al. 1997). For this particular afterglow, its non-detection has been attributed to a dust-lane in its host galaxy (Djorgovski et al. 2001). Dust extinction as the cause of the non-detection of the optical afterglow has been inferred in the case of several other GRBs, notably those with a precise X-ray or radio position, where one can pinpoint the afterglow position on top of its host galaxy (e.g. GRB 000210, Piro et al. 2002).

Optical drop-outs due to high redshift will also

result in dark bursts, but are harder to confirm, since it would require at least one detection in a red band, to detect the Ly α break. Otherwise, it becomes indistinguishable from dust extinction.

Other explanations of afterglow non-detections include the intrinsic faintness of the afterglow. For HETE-2 detected GRBs, this has been inferred for e.g. GRB 020819 (Jakobsson et al. 2005). For Swift bursts, where rapid and accurate X-ray positions are often available, this is a major cause of non-detections (Berger et al. 2005), largely attributed to a higher average redshift.

In our case here, the host galaxy has been detected at a relatively modest redshift, which almost automatically points to the dust extinction scenario. The radio and X-ray detections even allow us to accurately model the necessary amount of extinction between us and the GRB.

4.1. The burst environment

The issue of the role of dust extinction in the lines of sight towards GRBs is still very much an open one. While clear signs of dust depletion are seen in several afterglow spectra, the A_V values that are predicted from these depletion measures are generally much higher than the observed

ones, that can be found from the continuum shape (Savaglio & Fall 2004). Recently, selected samples of GRB afterglows were homogeneously analyzed for X-ray and optical extinction, showing dust to gas ratios different from Galactic and Magellanic cloud values (Starling et al. 2007; Schady et al. 2007). Galama & Wijers (2001) and Stratta et al. (2004) had already found dust (optical) to gas (X-ray) ratios to be lower than the Galactic value (in all cases, however, there is a bias in these samples to optically and X-ray detected afterglows). Comparison of neutral hydrogen columns and metallicities of afterglow lines of sight with X-ray extinction values (Watson et al. 2007) showed that the absorption probed by these two wavelength regimes is generally located at different positions in the host. In all these cases there may be significant biases against bursts with low apparent magnitudes, preventing optical spectroscopy, which are hard to quantify.

In the case of GRB 051022 there is a significant discrepancy between the extinction for the host as a whole and that along the line of sight to the burst, or at least along our line of sight towards the burst. This is perhaps not too surprising if one assumes, for example, that the burst occurred inside a Giant Molecular Cloud (GMC). Jakobsson et al. (2006a) compared the GRB $N(\text{HI})$ distribution to that of modeled GRBs located inside Galactic-like GMCs. They found that the two distributions are incompatible, and possibly GRBs are more likely to occur inside clouds with a lower $N(\text{HI})$, or alternatively, outside the actual GMC. (Note that their study concentrates on bursts with $z > 2$, where the Ly- α absorption is visible in the optical wavebands; it is also biased towards optically detected afterglows). A GMC could therefore actually be positioned in front of the GRB, where the required optical and X-ray extinction is easily achieved. This agrees with the findings by Prochaska et al. (2007), who analyzed several GRB-Damped Lyman Alpha spectra and from observed depletion levels infer that the gas is not located directly near the GRB (e.g. its molecular cloud) but further out. The specific case of GRB 060418 confirmed this through time-resolved high resolution spectroscopy, showing that the observed metal lines originate past 1.7 kpc from the burst itself (Vreeswijk et al. 2007). In fact, X-ray radiation from the burst could easily destroy

grains out to 100 pc (Waxman & Draine 2000; Fruchter et al. 2001; Draine & Hao 2002) and permit the afterglow radiation to penetrate the surrounding molecular cloud. Dust extinction is therefore likely to occur further out, perhaps to several kiloparsecs.

It is interesting to find a non-SMC type of extinction curve from the combination of X-ray and optical absorption (though not completely ruled out): in most cases modeled, an SMC extinction curve fits the optical-X-ray spectra best (Starling et al. 2007; Schady et al. 2007), presumably attributable to the absence of the 2175 Å feature (Savage & Mathis 1979) and the low dust to gas ratio. Our findings indicate that the extinction along the line of sight to the GRB will generally be different than one of the three assumed extinction curves. Local small scale density variations in clouds, such as found by from infrared studies in the Taurus region and from simulations (Padoan et al. 2006), could cause this fairly easily.

4.2. Energetics

Our modeling provides us with a detailed set of parameters of the afterglow energetics, including E_{jet} , the energy of the afterglow. For the prompt emission energy, we use the data from the Konus-Wind measurements (Golenetskii et al. 2005). We calculate a prompt isotropic energy of $4.39^{+0.29}_{-0.18} \times 10^{53}$ erg in the 20 keV – 20 MeV observer frame, and, by applying a K-correction (as in e.g. Bloom et al. 2001), $E_{\text{p,iso}} = 10.4^{+0.7}_{-0.4} \times 10^{53}$ erg in the $1 - 10^5$ keV rest frame. The collimation corrected energy depends on the assumed density profile of the surrounding medium: for a homogeneous medium, we obtain $E_{\text{p,jet}} = 18.2 \times 10^{50}$ erg, and for a wind-like medium, $E_{\text{p,jet}} = 8.38 \times 10^{50}$ erg. With $E_{\text{peak}} = 918^{+66}_{-59}$ keV in the burst rest frame, we find that the $E_{\text{peak}} - E_{\text{p,jet}}$ relation (Ghirlanda et al. 2004) somewhat underestimates the E_{peak} when calculated from $E_{\text{p,jet}}$: $E_{\text{peak}} \approx 740$ keV for a homogeneous medium, and ≈ 430 keV for a wind medium (the difference between our chosen cosmology and that used by Ghirlanda et al. 2004 amounts to only a 0.3% difference in E_{iso}). These estimates, however, come with a few caveats: 1) the E_{peak} from the Konus-Wind data is calculated using an exponential cut-off model, not the Band function (Band et al. 1993). Since the Band function includes the case of an expo-

nential cut-off model (with $\beta = -\infty$, this should, however, pose no problem in estimating the actual E_{peak}), 2) our break time, and therefore the jet-opening angle, are calculated from the full modeling of the afterglow, which effectively means derived from the available X-ray and radio data. Further, the original Ghirlanda relation was derived using optical break times. Recent efforts show that estimating jet-break times from X-ray light curves may not lead to the same results (e.g. Panaitescu et al. 2006), and 3) the relatively large error on the jet opening angle estimate allows for a relatively large range in collimation corrected energies. We have simply used here our best value, but an E_{peak} value of 1498 keV derived from E_{jet} can still be accommodated within our errors. (We note that, with a different E_{peak} estimate and an incorrect value for the jet-break time, Nakagawa et al. 2006 still found their results to lie on the Ghirlanda relation). The break time problem can be avoided by looking only at the $E_{\text{peak}} - E_{\text{p,iso}}$ relation (Amati et al. 2002; Amati 2006). From this, we estimate $E_{\text{peak}} \approx 924$ keV, nicely in agreement with the value found directly from the spectra fit.

Comparing the prompt emission energy ($E_{\text{p,jet}}$) and afterglow blast wave kinetic energy (E_{jet}), we find their ratio to be $E_{\text{p,jet}}/E_{\text{jet}} = 3.7$ in the case of a wind-like circumburst medium, while for a homogeneous medium, $E_{\text{p,jet}}/E_{\text{jet}} = 20$. These ratios are similar to those found for other bursts (e.g. Berger et al. 2003, Figure 3).

GRB 051022 is also one of the brightest bursts observed by HETE, with a prompt 30–400 keV fluence of $S = 1.31 \times 10^{-4}$ erg cm $^{-2}$ (Nakagawa et al. 2006). In fact, compared to the sample of 35 FREGATE bursts analyzed by Barraud et al. (2003), GRB 051022 has the largest fluence, even topping the relatively close-by GRB 030329 (Vanderspek et al. 2004, $S = 1.2 \times 10^{-4}$ erg cm $^{-2}$; note that for GRB 051022, its redshift is close to the median redshift of HETE-2 detected GRBs and therefore distance effects will play a very minor role). Rol et al. (2005) noted this potential correlation of fluence with the non-detection of a GRB afterglow for the small subset of genuinely dark bursts in their sample: the truly dark bursts all have a much higher than average fluence (although this is for a relatively small sample only). Potentially, this could point to an external origin for the prompt emission, instead of being due to

internal shocks: a large amount of dust may result in more matter that will radiate, while at the same time the radiation will be suppressed at UV and optical wavelengths. This would indicate an origin of the extinction quite close to the burst instead, in contrast to previous findings for other bursts, as discussed in Section 4.1. These latter bursts, however, were all optically selected to obtain spectroscopy, and may therefore show different surroundings than GRB 051022. Unfortunately, with the small sample size of genuine dark bursts a firm conclusion on this correlation is not possible, but remains something to watch for in future dark bursts.

5. Conclusions

GRB 051022 is a prototypical dark burst, with the local extinction exceeding 2.3 magnitudes in J and 5.4 magnitudes in U , in the host-galaxy restframe, with the exact limits depending on the circumburst density profile. The extinction curve derived from an X-ray – optical spectral fit points towards a Galactic type of extinction curve, although it is likely that this is more or less a coincidence: the host galaxy itself is best modeled with an SMC-like extinction curve, with a modest amount of extinction, $A_V \approx 1$ mag. The large optical absorption towards the afterglow of GRB 051022 is therefore probably the effect of an unfortunate position in the host where the line of sight crosses dense regions within the host.

The X-ray and radio afterglow data allow for a full solution of the blastwave model, although we unfortunately cannot distinguish between the density profile (homogeneous or wind-like) of the circumburst medium. We estimate a collimation-corrected energy in the afterglow emission of $0.92 - 2.3 \times 10^{50}$ erg, while the energy in prompt emission ($1 - 10^5$ keV rest frame) is $8.4 - 18 \times 10^{50}$ erg. Aside from the large optical extinction, the afterglow otherwise appears as an average afterglow, with no outstanding properties. The potentially interesting point here is that the 30–400 keV fluence of the prompt emission is one of the largest ever detected in the HETE-2 sample.

In the era of Swift GRBs, dust-extincted bursts can actually be found in optical/nIR thanks to the rapid availability of precise positions: examples are found where the burst is relatively bright early

on at optical/nIR wavelengths, while the afterglow proper (post few hours) often can go undetected (e.g. Oates et al. 2006; Perley et al. 2007). This allows targeted follow-up of such dark bursts, i.e. determining the host galaxy (and the bursts precise position therein) and a redshift measurement. In our case, a precise CXO and radio position pinpointed the host galaxy, but such data may not always be available. High resolution late-time observations of the host, at the location of the GRB, may then reveal whether the burst indeed occurred inside a dense host region.

We thank the referee for a careful reading of the manuscript and constructive comments. We thank Kim Page and Andy Beardmore for useful discussions regarding the XRT data analysis. ER and RLCS acknowledge support from PPARC. KW and RAMJW acknowledge support of NWO under grant 639.043.302. The authors acknowledge funding for the Swift mission in the UK by STFC, in the USA by NASA and in Italy by ASI. The Dark Cosmology Centre is funded by the Danish National Research Foundation. The William Herschel Telescope is operated on the island of La Palma by the Isaac Newton Group in the Spanish Observatorio del Roque de los Muchachos of the Instituto de Astrofísica de Canarias. The United Kingdom Infrared Telescope is operated by the Joint Astronomy Centre on behalf of the U.K. Particle Physics and Astronomy Research Council. The data reported here were obtained as part of the UKIRT Service Programme. The Westerbork Synthesis Radio Telescope is operated by ASTRON (Netherlands Foundation for Research in Astronomy) with support from the Netherlands Foundation for Scientific Research (NWO). Support for this work was provided by the National Aeronautics and Space Administration through Chandra Award Number 1736937 issued by the Chandra X-ray Observatory Center, which is operated by the Smithsonian Astrophysical Observatory for and on behalf of the National Aeronautics Space Administration under contract NAS8-03060. This publication makes use of data products from the Two Micron All Sky Survey, which is a joint project of the University of Massachusetts and the Infrared Processing and Analysis Center/California Institute of Technology, funded by the National Aeronautics and Space Administration and the National Science Foundation. This research has made use of data obtained from the High Energy Astrophysics Science Archive Research

Center (HEASARC), provided by NASA's Goddard Space Flight Center.

A. Interstellar scintillation in the radio modeling

The 4.9 GHz measurements show scatter around the best fit light curve, which can be accounted for by interstellar scintillation (ISS). In Figure 1 we have indicated the predicted rms scatter due to ISS. We have calculated the scattering measure from the Cordes & Lazio (2002) model for the Galactic distribution of free electrons: $SM = 2.04 \cdot 10^{-4} \text{ kpc/m}^{-20/3}$. The radio specific flux will be modulated when the source size is close to one of the three characteristic angular scales, i.e. for weak, refractive or diffractive ISS. From Walker (1998), we calculate the transition frequency between weak and strong ISS, $\nu_0 = 9.12 \text{ GHz}$, and the angular size of the first Fresnel zone, $\theta_{F_0} = 0.994 \mu\text{as}$. Our measurements were all performed at frequencies below ν_0 , i.e. in the strong ISS regime, which means that only refractive and diffractive ISS modulate the specific flux significantly. We calculate the evolution of the source size in the extreme relativistic phase ($\theta_s = R/\Gamma$) and after the jet-break ($\theta_s = R\theta_j$), and compare this source size with the diffractive angular scale $\theta_d = \theta_{F_0}(\nu_0/\nu)^{-6/5} = 0.0701 \cdot \nu_{\text{GHz}}^{6/5} \mu\text{as}$ and the refractive angular scale $\theta_r = \theta_{F_0}(\nu_0/\nu)^{11/5} = 128 \cdot \nu_{\text{GHz}}^{-11/5} \mu\text{as}$ to calculate the modulation index m_p . In the case of diffractive ISS the modulation index is 1, and in the case of refractive ISS $m_p = (\nu_0/\nu)^{-17/30} = 0.286 \cdot \nu_{\text{GHz}}^{17/30}$. Because of the expansion of the blastwave the angular source size exceeds one of the characteristic angular scales at some point in time. Then the modulation will begin to quench as $m_p(\theta_d/\theta_s)$ in the case of diffractive ISS, and as $m_p(\theta_r/\theta_s)^{7/6}$ in the case of refractive ISS.

REFERENCES

- Alard, C. 2000, *A&AS*, 144, 363
- Amati, L. 2006, *MNRAS*, 372, 233
- Amati, L., Frontera, F., Tavani, M., et al. 2002, *A&A*, 390, 81
- Arnaud, K. A. 1996, in *ASP Conf. Ser. 101: Astronomical Data Analysis Software and Systems V*, 17
- Band, D., Matteson, J., Ford, L., et al. 1993, *ApJ*, 413, 281
- Barraud, C., Olive, J.-F., Lestrade, J. P., et al. 2003, *A&A*, 400, 1021
- Berger, E., Kulkarni, S. R., Fox, D. B., et al. 2005, *ApJ*, 634, 501
- Berger, E., Kulkarni, S. R., Pooley, G., et al. 2003, *Nature*, 426, 154
- Berger, E. & Wyatt, P. 2005, *GCN Circular*, 4148
- Bloom, J. S., Frail, D. A., & Sari, R. 2001, *AJ*, 121, 2879
- Bolzonella, M., Miralles, J.-M., & Pelló, R. 2000, *A&A*, 363, 476
- Bremer, M., Castro-Tirado, A. J., & Neri, R. 2005, *GCN Circular*, 4157
- Butler, N. R., Ricker, G. R., Lamb, D. Q., et al. 2005a, *GCN Circular*, 4165
- . 2005b, *GCN Circular*, 4170
- Cameron, P. B. & Frail, D. A. 2005, *GCN Circular*, 4154
- Castro-Tirado, A. J., McBreen, S., Jelínek, M., et al. 2006, in *American Institute of Physics Conference Series*, Vol. 836, *Gamma-Ray Bursts in the Swift Era*, ed. S. S. Holt, N. Gehrels, & J. A. Nousek, 79–84
- Christensen, L., Hjorth, J., & Gorosabel, J. 2005, *ApJ*, 631, L29
- Cordes, J. M. & Lazio, T. J. W. 2002, *astro-ph/0207156*
- Dickey, J. M. & Lockman, F. J. 1990, *ARA&A*, 28, 215
- Djorgovski, S. G., Frail, D. A., Kulkarni, S. R., et al. 2001, *ApJ*, 562, 654
- Draine, B. T. & Hao, L. 2002, *ApJ*, 569, 780
- Evans, P. A., Beardmore, A. P., Page, K. L., et al. 2007, *A&A*, 469, 379
- Fitzpatrick, E. L. 1985, *ApJ*, 299, 219
- Fruchter, A., Krolik, J. H., & Rhoads, J. E. 2001, *ApJ*, 563, 597
- Fynbo, J. U., Jensen, B. L., Gorosabel, J., et al. 2001, *A&A*, 369, 373
- Gal-Yam, A., Berger, E., Fox, D. B., et al. 2005, *GCN Circular*, 4156
- Galama, T. J. & Wijers, R. A. M. J. 2001, *ApJ*, 549, L209
- Ghirlanda, G., Ghisellini, G., & Lazzati, D. 2004, *ApJ*, 616, 331
- Golenetskii, S., Aptekar, R., Mazets, E., et al. 2005, *GCN Circular*, 4150
- Groot, P. J., Galama, T. J., Van Paradijs, J., et al. 1998, *ApJ*, 493, L27
- Gunn, J. E. & Peterson, B. A. 1965, *ApJ*, 142, 1633
- Haislip, J. B., Nysewander, M. C., Reichart, D. E., et al. 2006, *Nature*, 440, 181
- Henden, A. 2005, *GCN Circular*, 4184, 1
- Jakobsson, P., Frail, D. A., Fox, D. B., et al. 2005, *ApJ*, 629, 45
- Jakobsson, P., Fynbo, J. P. U., Ledoux, C., et al. 2006a, *A&A*, 460, L13
- Jakobsson, P., Hjorth, J., Fynbo, J. P. U., et al. 2004, *ApJ*, 617, L21
- Jakobsson, P., Levan, A., Fynbo, J. P. U., et al. 2006b, *A&A*, 447, 897
- Jester, S., Schneider, D. P., Richards, G. T., et al. 2005, *AJ*, 130, 873
- Levan, A., Fruchter, A., Rhoads, J., et al. 2006, *ApJ*, 647, 471

- Lin, L., Koo, D. C., Weiner, B. J., et al. 2007, *ApJ*, 660, L51
- Martin, N., Maurice, E., & Lequeux, J. 1989, *A&A*, 215, 219
- Nakagawa, Y. E., Yoshida, A., Sugita, S., et al. 2006, *PASJ*, 58, L35
- Oates, S. R., Mundell, C. G., Piranomonte, S., et al. 2006, *MNRAS*, 372, 327
- Odewahn, S. C., Djorgovski, S. G., Kulkarni, S. R., et al. 1997, *IAU Circ.*, 6735, 1
- Oke, J. B. & Gunn, J. E. 1983, *ApJ*, 266, 713
- Olive, J., Ricker, G., Atteia, J., et al. 2005, *GCN Circular*, 4131
- Ovaldsen, J. ., Jaunsen, A. O., Fynbo, J. P. U., et al. 2007, *ApJ*, 662, 294
- Padoan, P., Cambr sy, L., Juvela, M., et al. 2006, *ApJ*, 649, 807
- Panaiteacu, A. & Kumar, P. 2001, *ApJ*, 560, L49
- Panaiteacu, A., M sz ros, P., Burrows, D., et al. 2006, *MNRAS*, 369, 2059
- Patel, S., Kouveliotou, C., & Rol, E. 2005, *GCN Circular*, 4163
- Pe’er, A. & Wijers, R. A. M. J. 2006, *ApJ*, 643, 1036
- Pei, Y. C. 1992, *ApJ*, 395, 130
- Perley, D. A., Bloom, J. S., Butler, N. R., et al. 2007, *astro-ph/0703538*
- Piro, L., Frail, D. A., Gorosabel, J., et al. 2002, *ApJ*, 577, 680
- Predehl, P. & Schmitt, J. H. M. M. 1995, *A&A*, 293, 889
- Prochaska, J. X., Chen, H.-W., Dessauges-Zavadsky, M., & Bloom, J. S. 2007, *ApJ*, submitted
- Racusin, J., Burrows, D., & Gehrels, N. 2005a, *GCN Circular*, 4141
- Racusin, J., Kennea, J., Fox, D., et al. 2005b, *GCN Circular*, 4169
- Rhoads, J. E. 1997, *ApJ*, 487, L1
- Ricker, G. R., Atteia, J.-L., Crew, G. B., et al. 2003, in *American Institute of Physics Conference Series*, Vol. 662, *Gamma-Ray Burst and Afterglow Astronomy 2001: A Workshop Celebrating the First Year of the HETE Mission*, ed. G. R. Ricker & R. K. Vanderspek, 3–16
- Rol, E., Osborne, J. P., Page, K. L., et al. 2007, *MNRAS*, 374, 1078
- Rol, E., Wijers, R. A. M. J., Kouveliotou, C., Kaper, L., & Kaneko, Y. 2005, *ApJ*, 624, 868
- Savage, B. D. & Mathis, J. S. 1979, *ARA&A*, 17, 73
- Savaglio, S. & Fall, S. M. 2004, *ApJ*, 614, 293
- Schady, P., Mason, K. O., Page, M. J., et al. 2007, *MNRAS*, 377, 273
- Schaefer, B. E. 2005, *GCN Circular*, 4132
- Schlegel, D. J., Finkbeiner, D. P., & Davis, M. 1998, *ApJ*, 500, 525
- Skrutskie, M. F., Cutri, R. M., Stiening, R., et al. 2006, *AJ*, 131, 1163
- Starling, R. L. C., Wijers, R. A. M. J., Wiersema, K., et al. 2007, *ApJ*, 661, 787
- Stratta, G., Fiore, F., Antonelli, L. A., Piro, L., & De Pasquale, M. 2004, *ApJ*, 608, 846
- Tan, G. H. 1991, in *Astronomical Society of the Pacific Conference Series*, Vol. 19, *IAU Colloq. 131: Radio Interferometry. Theory, Techniques, and Applications*, ed. T. J. Cornwell & R. A. Perley, 42–46
- Tanvir, N. R., Barnard, V. E., Blain, A. W., et al. 2004, *MNRAS*, 352, 1073
- Tody, D. 1986, in *Instrumentation in astronomy VI; Proceedings of the Meeting*, Tucson, AZ, Mar. 4-8, 1986. Part 2 (A87-36376 15-35). Bellingham, WA, Society of Photo-Optical Instrumentation Engineers, 1986, p. 733., 733
- Tokunaga, A. T. & Vacca, W. D. 2005, *PASP*, 117, 421
- Torii, K. 2005, *GCN Circular*, 4130

- Trentham, N., Ramirez-Ruiz, E., & Blain, A. W.
2002, MNRAS, 334, 983
- van der Horst, A., Wijers, R. A. M. J., & van der
Horn, L. 2007, A&A, submitted
- Van der Horst, A. J., Rol, E., & Wijers, R. A. M. J.
2005, GCN Circular, 4158
- Vanderspek, R., Sakamoto, T., Barraud, C., et al.
2004, ApJ, 617, 1251
- Vreeswijk, P. M., Ledoux, C., Smette, A., et al.
2007, A&A, 468, 83
- Walker, M. A. 1998, MNRAS, 294, 307
- Watson, D., Hjorth, J., Fynbo, J. P. U., et al.
2007, ApJ, 660, L101
- Waxman, E. & Draine, B. T. 2000, ApJ, 537, 796
- Yost, S. A., Harrison, F. A., Sari, R., & Frail,
D. A. 2003, ApJ, 597, 459